

# Numerical Optimization of Thrust Efficiency of Propulsion in Fluid using a Fin with Variable Stiffness

Masataka Nakabayashi,<sup>a,\*</sup> Yusuke Yamaguchi<sup>b</sup> and Wataru Yamazaki<sup>c</sup>

<sup>a</sup> Graduate School of Engineering, Utsunomiya University, Japan

<sup>b</sup> Advanced Engineering Services, Co., Ltd, Japan

<sup>c</sup> Department of Mechanical Engineering, Nagaoka University of Technology, Japan

*Abstract*—Underwater propulsion using a flexible elastic fin that mimics fish locomotion is investigated. Because the degree of elasticity is important for thrust efficiency, a fin with a dynamic variable-effective-length spring as a variable-stiffness mechanism is experimentally analyzed. The yawing of the elastic fin in still water is simulated using fluid–structure interaction analysis. There is a clear relationship between the effective length of the spring and Young’s modulus for the dynamic stiffness of the fin. Additionally, using the kriging surface response approach, thrust efficiency is demonstrated to be better under dynamic conditions.

*Index Terms*—Propulsion mechanism, Fin with variable stiffness, Fluid–structure interaction, Numerical optimization.

## I. INTRODUCTION

The mechanism of fluid propulsion widely used for general ocean vessels is the screw propeller. For (micro-) unmanned ocean vessels, however, propulsion using elastic fins that mimic fish locomotion is being watched with keen interest. A number of experimental studies on fish locomotion have documented its use in ships or underwater vehicles/robots: e.g., the tuna robot [1], dolphin robot [2], fish robot [3], bio-inspired elastic fin [4], and bio-inspired robots for research on the stiffness of fish [5]. In the numerical study of propulsion of a fish robot using fluid–structure interaction (FSI) analysis in computational fluid dynamics (CFD), the effects of tail-fin flexibility on the propulsive force were investigated [6][7]. One of the advantages of this type of propulsion is its capability of locomotion without agitating debris from the sea bottom. Moreover, another major advantage is the lower risk of harming aquatic life.

The optimum elasticity of a fin modeled on the caudal fin for propulsion is not constant and changes with swimming speed and task. However, replacing a fin of different stiffness while moving is very difficult. For this reason, a fin with a dynamic varying-effective-length spring that can change its stiffness during oscillatory

motion was developed and experimentally investigated [8][9][10].

In our previous paper, we measured the thrust and the lateral forces of the propulsion mechanism for this fin in a quasi-two-dimensional (2D) water tank. Furthermore, 2D FSI analyses were performed under static conditions for which the effective length of the spring was fixed at certain values during the oscillatory movement. Qualitative agreement was observed between the FSI analyses and the experimental results from the quasi-2D environment [11].

However, the dynamic conditions under which the fin was subjected, i.e., the effective length of the spring (corresponding to the apparent fin stiffness) changed during the oscillatory motion. Indeed, in an attempt to enhance propulsive performance, control of the dynamic stiffness of the fin was difficult with the method used in our previous numerical study because the grid information of the fin changed dynamically, rendering the numerical analysis unstable.

Therefore, in this paper, the relationship between the effective length of the spring and Young’s modulus is clarified using FSI simulations. Additionally, based on these results, a 2D FSI analysis was able to be performed under dynamic conditions. We describe how we achieved optimal control of the dynamic stiffness of the fin to attain maximum thrust efficiency using the kriging response surface approach.

## II. PRINCIPLE OF THE FIN WITH A DYNAMIC VARIABLE EFFECTIVE LENGTH SPRING

The principle underlying the variable-effective-length spring is schematically shown in Fig. 1. The elastic portion is a plate made from polyethylene terephthalate (PET), which is then sandwiched between two rigid brass plates. By exposing a length of the PET plate ( $H$  in Fig. 1), the apparent fin stiffness can be dynamically changed. Figure 2 shows the fin with the variable-effective-length spring. The fin system consists of an aluminum box (length: 130 mm, height: 60 mm, width: 25 mm), a fin made of a chloride plate (length: 120 mm), and a variable-effective-length spring (length  $L$ : 20 mm, height: 60 mm, thickness: 0.5 mm).

\* Corresponding author: 7-1-2 Yoto, Utsunomiya 321-8585, Japan, E-mail: m\_nakabayashi@cc.utsunomiya-u.ac.jp.

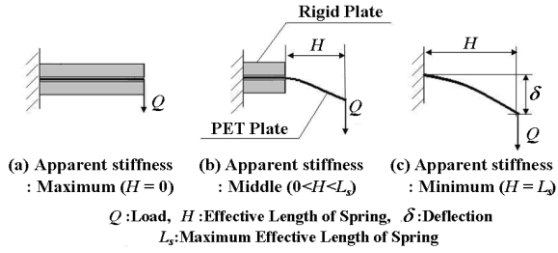


Fig. 1. Principle behind the variable-effective-length spring

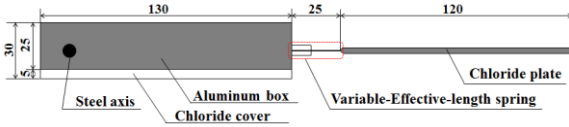


Fig. 2. Fin with variable-effective-length spring

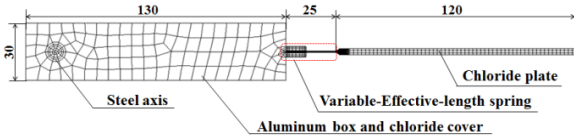


Fig. 3. Computational grid for structural analysis of the fin with variable-effective-length spring

In this study, the exposed length of the PET plate is changed from 0 mm (most rigid) to 20 mm (most elastic). We noted just the thrust characteristics of the fin as the only propulsor in the fluid. The thrust characteristics of fin yawing without considering the bio/fish robot body have been studied [8][9][10]. This study investigated the thrust characteristics and flow field around the fin in the same manner as described in our previous papers.

### III. ANALYSIS METHOD

#### A. Analysis Model

The FSI analyses of the flexible fin were performed using ANSYS CFX 13.0 (for fluid) and ANSYS Mechanical 13.0 (for structure). The 2D model of the fin for structural deformation analysis is shown in Fig. 3. The object domain and computational grids around the fin for the analysis of the fluid are shown in Figs. 4 and 5. These models were used in our previous study [11], and hence are only briefly described here.

In regard to the computational fluid analysis, the governing equations are the Navier–Stokes (NS) equation and the equation of continuity; the advection scheme is the secondary accuracy upwind scheme and the standard  $k-\varepsilon$  turbulence model has also been adopted. For the governing equation for computational structure analysis, the constitutive equation of linear elastic body has been chosen.

With maximum yawing angle  $\theta_{\max}$  and oscillating cycle set at  $30^\circ$  and 3 sec, respectively, a yawing motion is applied to the elastic fin, for which the motion is

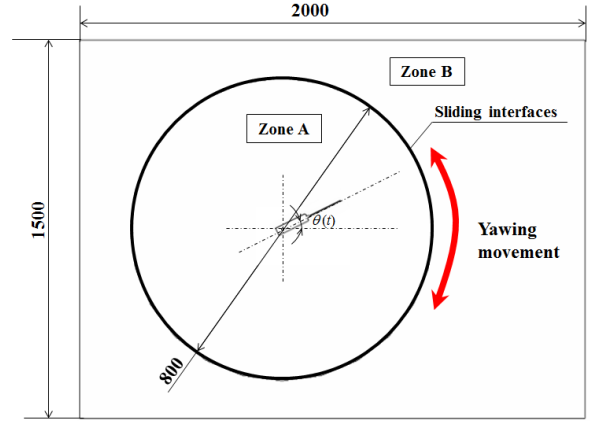


Fig. 4 Constitution of the objective domain around the fin and the coordinate system.

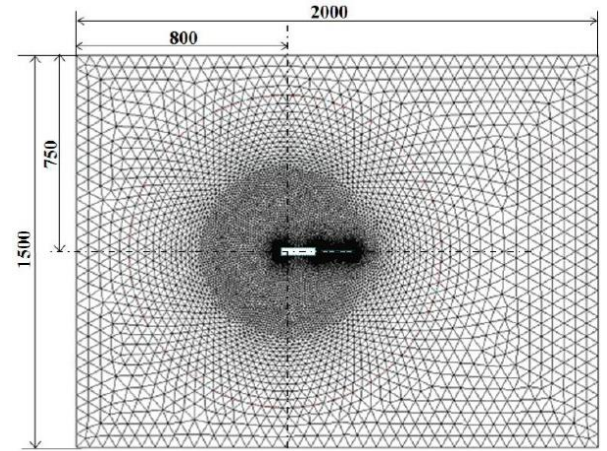


Fig. 5. Computational grids around the fin for the 2D FSI analysis

defined by a sin wave [11]. This motion is performed computationally by moving the domain of zone A in Fig. 4. The FSI simulation is performed in the object domain specified as still water (length: 2000 mm, width: 1500 mm, depth: 60 mm). Because the calculated value for the initial term of the analysis was unstable, the evaluation of the reciprocating movement was begun after approximately a quarter cycle (time step = 0 – 0.74 sec). A cycle is then defined as the phase  $\psi = 360^\circ$  with  $\theta(\psi)$  determining the yawing angle.

#### B. Settings in Changing the Fin's Stiffness

We defined two control conditions for the stiffness of the fin. One is a static condition for which the fin stiffness is fixed at each step during yawing motion. The other is a dynamic condition that the fin stiffness is changed during yawing motion to improve thrust performance [9][10]. In our previous numerical study, the apparent fin stiffness had been evaluated by the effective length of the spring  $H$ . However, the computational grid information of the fin varies according to the effective length of the spring [11]. The change in the computational grid information occurs under a dynamic condition, and therefore a problem arises over the reliability of the data because uniformity of the numerical calculation is lost. Accordingly, an alternative simulation method is proposed in which the



Fig. 6. Definitions of the half-cycle stages in yawing movement

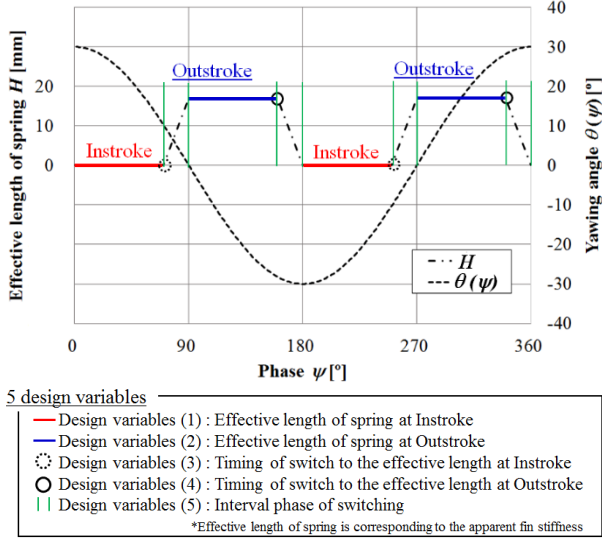


Fig. 7. Profile of fin stiffness and definitions of design variables

stiffness of the effective length of the spring is changed without varying the grid information. Therefore, we propose a simulation method where the portion of the variable effective length of the spring is determined dynamically using Young's modulus through the setting of values for physical properties in ANSYS Mechanical. The relationship between the effective length of the spring and Young's modulus are clarified by comparing the simulation results in our previous paper [11] with those changes in Young's modulus performed without changing grid information under static conditions. The results of these simulations are described below. The structural and fluid models used in these simulations were the same as those in previous paper with condition  $H = 3$  mm [11]. The number of nodes and the number of elements in the computational grid for fluid analysis are 45498 and 65471, respectively, and those for the structural analysis are 11491 and 1995.

### C. Evaluation of Thrust Efficiency

In our previous experimental study, an evaluation of the thrust efficiency was obtained using the torque, angular velocity, thrust force, and characteristic length of the yawing motion of the fin [9]. Nevertheless, it is difficult to establish a value in ANSYS Mechanical and CFX. Therefore, in this study, the thrust efficiency  $E$  of propulsion mechanism is defined as

$$E = \frac{\overline{P}_{out}}{\overline{P}_{in}} = \frac{\overline{F}_T V_\infty}{M\omega} = \frac{\overline{F}_T}{M\omega}, \quad (1)$$

where  $\overline{P}_{out}$  and  $\overline{P}_{in}$  are respectively the averaged thrust power and averaged required power per cycle;  $\overline{F}_T$  is the average thrust force;  $V_\infty$  is characteristic velocity, which

for convenience is set equal to 1 m/s;  $M$  is the moment acting on the center of rotation of the fin; and  $\omega$  is the angular velocity of the yawing movement. Moreover, this thrust efficiency is defined without considering the power required in controlling fin stiffness.

### D. Optimization Approach in Dynamic Conditions

#### 1) Kriging Response Surface Approach for Optimizing Thrust Efficiency

The stiffness control of the fin is optimized while dynamic conditions are imposed. In this study, we used the kriging response surface approach for this optimization [12][13]. First, the initial sample points are generated in the design variable space using the Latin hypercube sampling method, and then these are evaluated by CFD computations. The search of a promising location in the design variable space is executed by a genetic algorithm. This location is explored by the criteria of expected improvement ( $EI$ ) [12]. The CFD computation is performed for the candidate location (configuration) where  $EI$  is maximal, and then new models are created by adding its information. By the iterative process above, the accuracies of the models are efficiently increased around the candidate locations in the design variable space. The design variables and the objective function used in this study are defined in the next section.

#### 2) Design Variables and Objective Function

In this section, we introduce the definitions of the design variables stated for the dynamic conditions. For the dynamic change in stiffness, the change in stiffness over one cycle has to be determined. For this purpose, the yawing motion of the fin was divided into two stages: the instroke where the central axis of aluminum box of the fin moves toward the center from outside (see Fig. 6(a)), and the outstroke for which the motion begins at the center and moves outward (see Fig. 6(b)). For these two motions, five design variables describing the dynamic conditions were identified (Fig. 7). The effective length of the spring is established using settings of the physical properties in ANSYS Mechanical (see Section III.B). Design variables (1) and (2) are the effective lengths of the spring (corresponding to its Young's modulus) for the instroke and outstroke, respectively (The range of effective length of the spring is  $H = 0 - 20$  mm). Design variables (3) and (4) are for the timing in switching the effective length of the spring for the instroke and for the outstroke. Design variable (3) is fixed at the reference point phase  $\psi = 90^\circ, 270^\circ$  and (4) is fixed at  $\psi = 180^\circ, 360^\circ$ . The variable range of these design variables is set at  $\pm 20^\circ$  so as not to interfere with the switching phase between the inward and outward phases. Design variable (5) is the interval phase for switching, which is the total phase required in switching the effective length of the spring. The range of values is determined from the minimum range of  $\pm 9.6^\circ$  and the maximum range of  $\pm 19.6^\circ$ , which were established in the performance analysis of the experimental device used in our previous study[8][9]. There we also determined that

the objective function that requires maximization is the thrust efficiency given in Eq. (1).

#### IV. RESULTS AND DISCUSSION

##### A. Static Condition

##### 1) Thrust and Lateral Forces under Static Conditions

Figure 8 shows a comparison between simulation results obtained under static conditions in which grid information changed when fin stiffness was varied (broken line) and for which grid information was not changed and the stiffness was varied using the settings of physical properties in ANSYS Mechanical (solid line). These graphs (a) and (b) show the changes in thrust force  $F_T$  and lateral force  $F_L$  under static conditions over one cycle. The simulation results were obtained using settings of the physical properties obtained through trial and error. To reduce computational costs, the total calculation time for each static condition was 1.3 cycles, with the evaluations taken over a full cycle beginning after 0.25 cycles into the computation. From the two simulations, the amplitudes of  $F_T$  and  $F_L$  decrease with increasing  $H$ , as in our previous report [11]. A qualitative agreement is seen between the results for both simulation methods. From these results, it seems that the apparent stiffness of the variable-effective-length spring can be represented by Young's modulus using the setting of

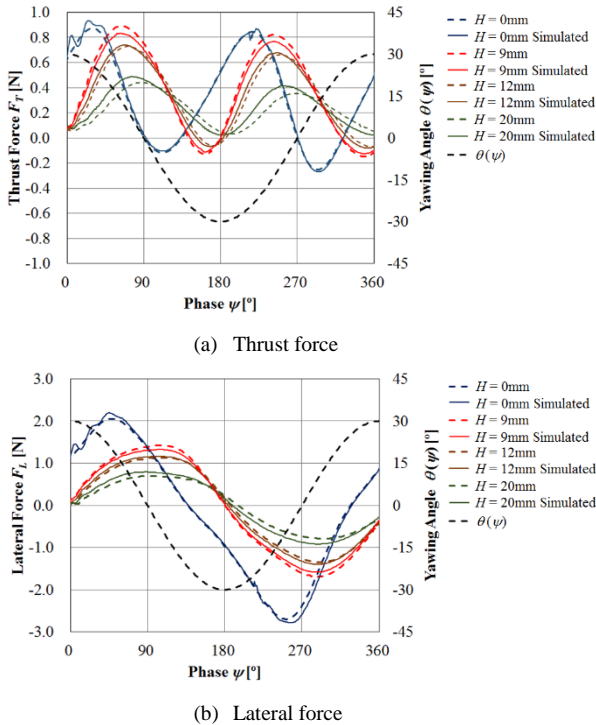


Fig. 8. Comparison between full-cycle simulation results obtained with various fin stiffnesses and grid information and those obtained without varying the grid information employing settings of physical properties for static condition.

Table 1 Relationship between effective length of the spring and Young's modulus

Effective length of spring $H$ [mm]	Young's modulus $E$ [GPa]
0	5.00
3	1.10
6	0.50
9	0.30
12	0.25
15	0.20
20	0.15

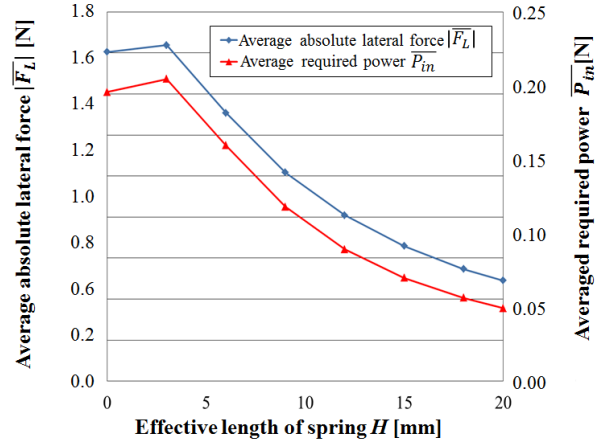


Fig. 9. Average absolute lateral force  $|F_L|$  and average required power  $P_{in}$  as a function of the effective length of the spring  $H$ .

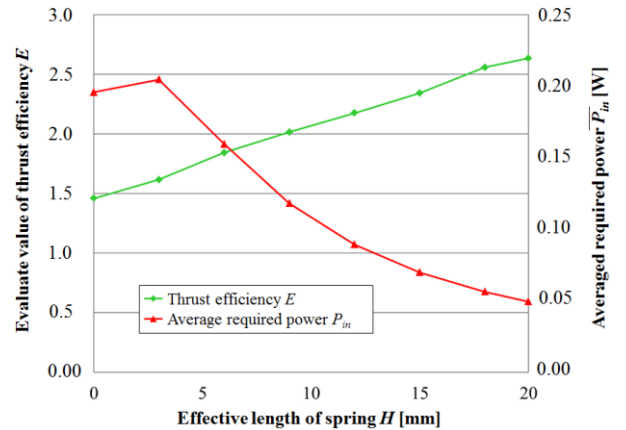


Fig. 10. Dependence of thrust efficiency  $E$  and average required power  $P_{in}$  on the effective length of a spring.

the physical properties. Table 1 gives the relationship between the effective length of the spring and Young's modulus obtained from the above simulations. Using these data, a simulation under dynamic conditions was performed. Below we discuss the thrust characteristics of only the fin as described in Section II. When the fin is attached to the bio/fish robot, the fluid force exerted (thrust and lateral force) was found to be quantitatively reduced by the drag being generated around the robot body. In a numerical study that took into account the main body in the propulsion mechanism [14], the presence of the body was found not to contribute significantly to propulsion. The results of that analysis suggests that they are qualitatively similar to those obtained in this current study.

2) Average Absolute Lateral force and Average Required Power in Static Condition

The average absolute lateral force  $|\overline{F_L}|$  and the average required power  $\overline{P_{in}}$  as functions of  $H$  under static conditions (Fig. 9) show a decreasing trend. This trend is the same as previously reported, although the definition of  $\overline{P_{in}}$  differs from our previous paper [9]. The reason given is that the fluid force acting on the fin decreases because of a decrease in fin stiffness when  $H$  is decreased. Power  $\overline{P_{in}}$  depends on the moment generated around the fin, which is equivalent to the lateral force. Hence, it seems appropriate for these simulation results because a qualitative agreement is observed between the trends for  $\overline{P_{in}}$  and  $|\overline{F_L}|$  as  $H$  is varied.

3) Average Required Power and Thrust Efficiency under Static Conditions

Variations of both thrust efficiency  $E$  and  $\overline{P_{in}}$  as functions of  $H$  under static conditions are given (Fig. 10). These values of  $E$  and  $\overline{P_{in}}$  are defined in Section III.C.  $E$  increases with increasing  $H$ ; recall that an increase in  $H$  means a decrease in fin stiffness. Contrary to this result,  $\overline{P_{in}}$  decreases with increasing  $H$  as described in Section IV.A.2. Considering these results, the reason for the trends seems to be that the rate of force in the direction of propulsion increases relatively with decreasing fin stiffness. This occurs despite the generated fluid forces (thrust and lateral forces,  $F_T$  and  $F_L$ ) decreasing with decreasing fin stiffness because the rate of change of the lateral force decreases during the elastic bending of the fin.

B. Dynamic Condition

1) Optimize Results

Figure 11 shows the relationship between  $E$  and  $\overline{F_T}$  obtained using the kriging method in all cases. The eight blue data points represent simulation results obtained under static conditions; the 16 green data points represent results obtained using combinations of the five design variables chosen randomly using Latin hypercube sampling. Finally, the 18 red data points represent optimized results obtained using the iterative calculation

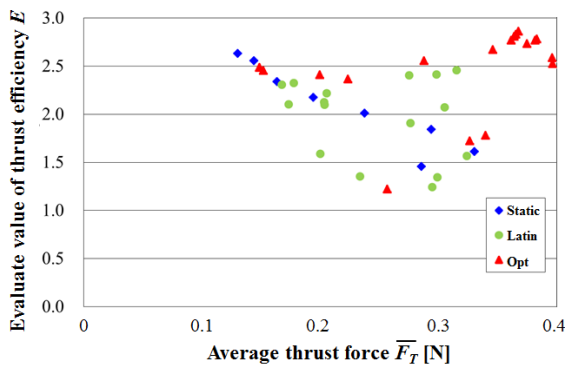
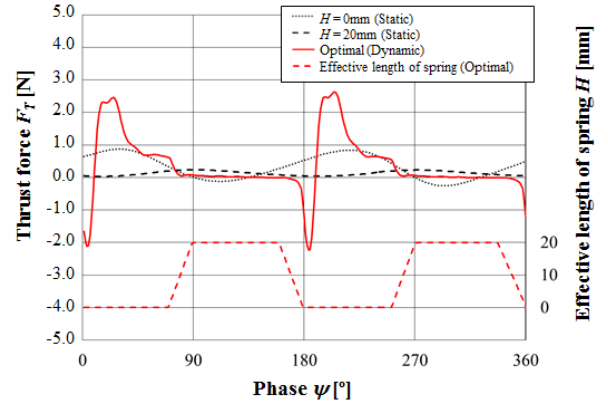
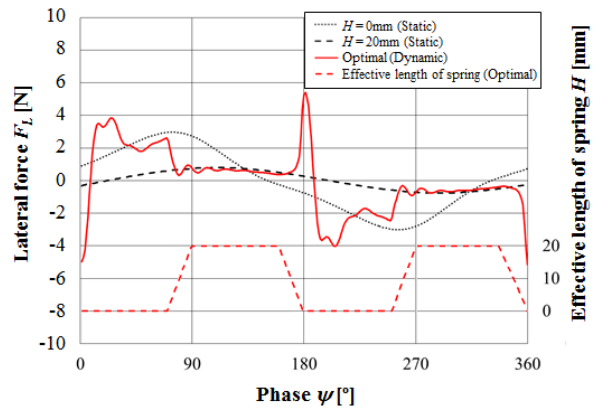


Fig. 11. Optimize results obtained by Latin hypercube sampling and the kriging methods



(a) Thrust force



(b) Lateral force

Fig. 12. Variation of fluid forces in dynamic conditions optimized using the kriging and gene algorithm methods

of the kriging method as described in Section III.D.1; they were based on the information for the 16 data points obtained by Latin hypercube sampling.

The full calculation for each condition represented 2.25 cycles, with the evaluation of fluid force taken over one complete cycle beginning at 1.25 cycles, to obtain a more reliable value from the analysis. Considering these results for the static condition, larger values for the calculated  $E$  generated smaller values for  $\overline{F_T}$ . From these results, it is apparent that a trade-off exists between these two variables. Nevertheless, the values of both  $\overline{F_T}$  and  $E$  for the optimize results were large compared with those from the static condition, and therefore indicating that both values can be improved under dynamic conditions.

2) Optimized Stiffness Control of the Fin

From the optimize results obtained using the kriging method, the variation in  $H$  under dynamic conditions at maximum  $E$  were plotted (red broken line in Fig. 12(a) and (b)). Design variables (1) and (2) exhibited a minimum value ( $H=0$  mm) and a maximum value ( $H=20$  mm), respectively. For the design variables (3) and (4), both have values of less than  $20^\circ$  from reference phases ( $\psi = 90^\circ, 180^\circ, 270^\circ, 360^\circ$ ) described in Section III.D.2. The optimized value of design variable (5) is  $19.6^\circ$ , which is the lowest of the set.

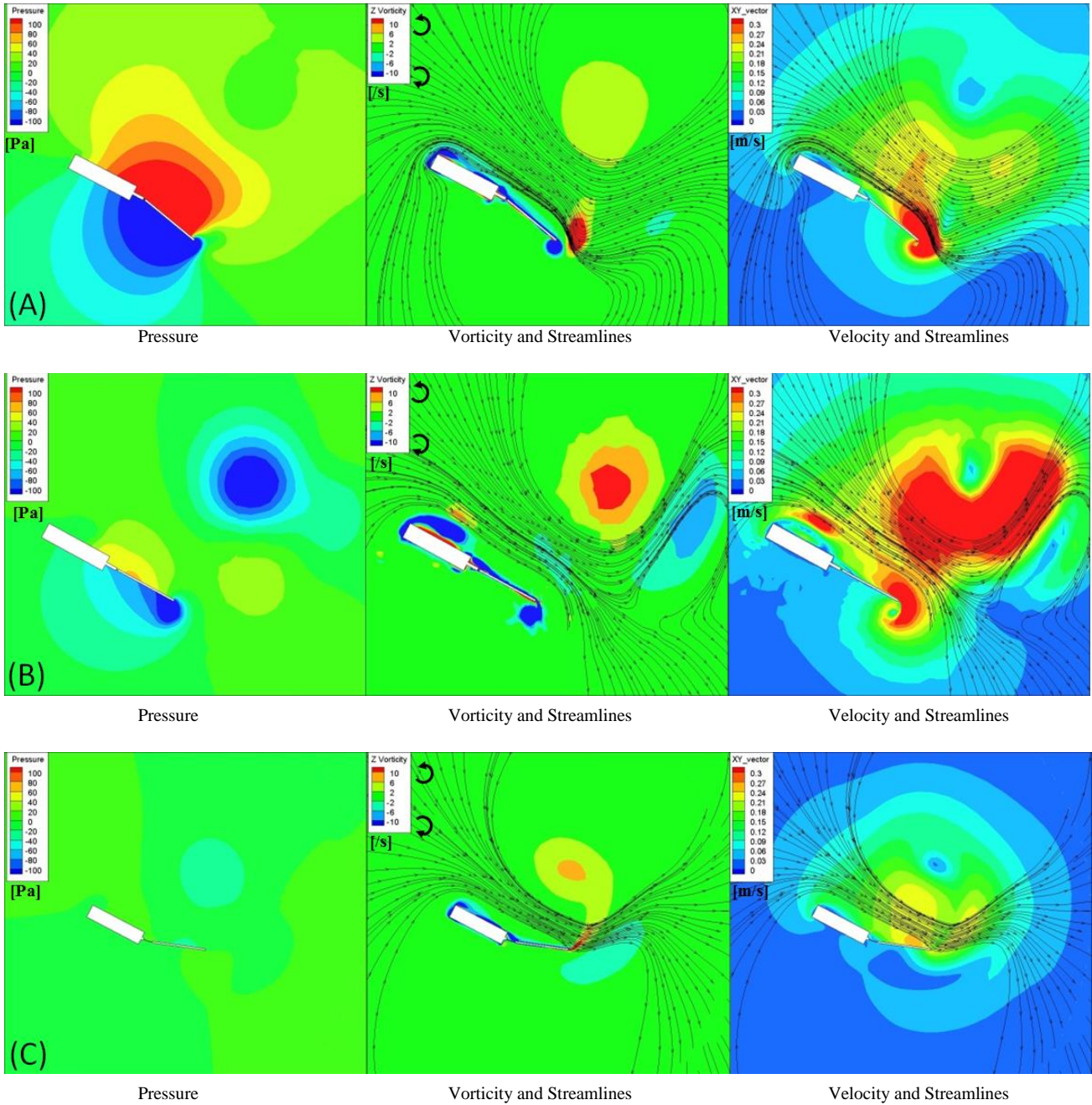


Fig. 13. Distributions around the fin of (left) pressure, (center) vorticity with streamlines, and (right) absolute value of flow velocity with streamline in (A) optimal dynamic conditions and (B) static conditions with  $H=0$  mm, and (C) static conditions at  $H=20$  mm (Phase  $\psi=203^\circ$ )

### 3) Thrust Force, Lateral Force in Optimal Dynamic Condition

Figure 12(a) shows the variation in thrust force under optimized dynamic (red line) and static conditions for  $H = 0$  mm and 20 mm. The phase intervals at which the peak of the positive thrust force is generated are  $\psi = 0^\circ - 90^\circ$  and  $180^\circ - 270^\circ$ . The peak in the positive thrust under optimal dynamic condition obtained using the kriging method was larger than those obtained under static conditions. The reason is that the fluid force acting on the fin is increased on increasing the fin stiffness during the instroke. Figure 13(A) shows flow visualization results for  $\psi = 203^\circ$  when the maximum

thrust force is generated under optimal dynamic condition; Figs. 13(B) and (C) similarly show results for  $H = 0$  mm and 20 mm under static conditions. The distributions of pressure, vorticity, and the absolute value of the flow velocity, as well as streamlines around the fin, are shown. With  $H = 20$  mm [see Fig. 13(C)], the shape of the fin and the flow field were observed to be different from that for other condition [Figs. 13(A) and (B)]; the shape and flow field is similar to that for an outstroke. The reason is that the bending angle of the fin increases with decreasing fin stiffness, because of the fluid force exerted on the fin, and the delay in the phase of the wave form for the bending angle from a decreasing fin stiffness, as reported previously [11]. During the instroke, the fin remains bent towards the center from the

fluid force occurring in the outstroke of the previous phase. From the results under static conditions with  $H = 0$  mm [Fig. 13(B)], the flow field under a maximum stiffness is seen to generate a high flow velocity behind the tip of the fin. For this reason the fluid is pushed strongly in the reverse direction to the direction of propulsion without the fin bending. Moreover, the field produces a high pressure zone comparable with that for  $H = 20$  mm [Fig. 13(C)], i.e., the minimum stiffness around the fin. In this field, a laterally directed flow occurs with the appearance of two counter-rotating vortices from the previous instroke, similar to results previously reported [11]. In this situation, the effective force of propulsion is believed to have decreased. Also, from the results obtained under static condition with  $H = 20$  mm, an induced flow effecting the propulsion direction is formed by the two vortices at the tip of the fin during the outstroke, caused by the bending fin [11]. This phenomenon is seen in Fig. 13(C). For this reason, the negative thrust force presumably is suppressed under static conditions with  $H = 20$  mm compared with that under static conditions with  $H = 0$  mm during the outstroke.

Under optimal dynamic condition [Fig. 13(A)], the induce flow appears to effect propulsion when the fin stiffness decreases during the outstroke, by switching the instroke, the fin pushes the fluid further in the reverse direction to the propulsion by increasing the fin stiffness. From the various distributions of pressure, vorticity, flow velocity, and streamlines, the positive value of the pressure and the reverse flow velocity opposing the force of propulsion in the central side of the fin are larger than in those of other static conditions. The direction of the streamlines formed by the vortex pair behind the tip of the fin [upper side in Fig. 13(A) (right)] were aligned with the direction of propulsion supporting the above considerations. From these factors, the instantaneous thrust force under optimal dynamic condition was larger than that in other static conditions.

However, large negative thrust force occurs near phases  $\psi = 0^\circ, 180^\circ$  under optimal dynamic condition [Fig. 12(a)]. The reason seems to arise from a combination of design variables (3), (4), and (5). In optimal stiffness control of the fin obtained by the kriging method, both timings for the switching of the effective length of the spring at instroke and outstroke (associated with design variables (3) and (4)) occur at values before  $20^\circ$  from the reference phases of  $\psi = 90$  ( $270^\circ$ ) and  $180$  ( $360^\circ$ ); i.e., these optimal timings correspond to phases  $\psi = 70$  ( $250^\circ$ ),  $160$  ( $340^\circ$ ). Despite using this optimal stiffness control, a large negative thrust force was instantaneously generated in the neighboring phases of  $\psi = 0^\circ, 180^\circ$  (the latter for the outstroke). The reason seems to be that the large fluid force of the reverse direction of propulsion occurred because the fluid force generated with the previous instroke cannot be turned aside, for the reason that the

timing of the switch over to high fin stiffness is too early for the outstroke.

Regarding the variation of lateral force, both large positive and large negative lateral forces are generated in the instroke (phases  $\psi = 0^\circ-90^\circ, 180^\circ-270^\circ$ ). The reason is that a large fluid force is generated around the fin because the fin stiffness is high during these phases. Nevertheless, the value of the lateral force was suppressed in the outstroke (phases  $\psi = 90^\circ-160^\circ, 270^\circ-350^\circ$ ), for which the value is close to that under static conditions with  $H = 20$  mm when the amplitude of the lateral force is a minimum. In regard to these results, the fluid force appears to be turned aside with the bending of the fin because the fin stiffness is small in the outstroke. Also, it was observed that the value of the large lateral force in the neighboring phases of  $\psi = 180$  ( $0, 360^\circ$ ) occurs locally. The reason is believed to be the same as that for the thrust force.

In this paper, the flow field around the fin was analyzed without considering the main body of the bio/fish robot. From the results of the study of the effects of tail-fin flexibility on the performance in propulsion of small fish-like robots [6] and the numerical investigations of the hydrodynamics of carangiform swimming [15], the main flow of fluid that affected the motion of the main body was generated around the fin and tail while generating a boundary layer along the main body. From these research reports analyzing the main body of a bio/fish robot with an attached fin, the generated boundary layer along the main body and the flow field are similar to the results of our analysis presented above.

#### 4) *Optimal and Comparative Dynamic Conditions*

From the results for the optimal dynamic condition obtained by the kriging method, large values for the negative thrust force and for the lateral force are observed to occur locally. The reason is because the timing of the switch to higher fin stiffness is too early, as described in Section IV.B.3. The timing of the switch to the effective length of the spring (corresponding to the design variable (4)) was then set at its slowest value (Phase  $\psi = +20^\circ$ ) to suppress the large negative thrust force. This setting defines the comparative dynamic condition. A FSI analysis for this setting was performed beginning with the variation of thrust and lateral force (Fig. 14). A large negative thrust force is suppressed near phases  $\psi = 180$  ( $0, 360^\circ$ ). This result was expected as the fin can turn aside the fluid force by delaying the timing of the switch of the effective length during the outstroke.

Table 2 lists the average thrust force  $\overline{F_T}$ , the average required power  $\overline{P_n}$  and the efficiency  $E$  under static conditions ( $H = 3, 20$  mm) and dynamic conditions. With  $H = 3$  mm, the largest average thrust force was generated. Values of  $\overline{F_T}$  and  $E$  under dynamic conditions were larger those under static conditions. From this comparison, control through dynamic stiffness of the fin is more effective. Also, although the large negative thrust

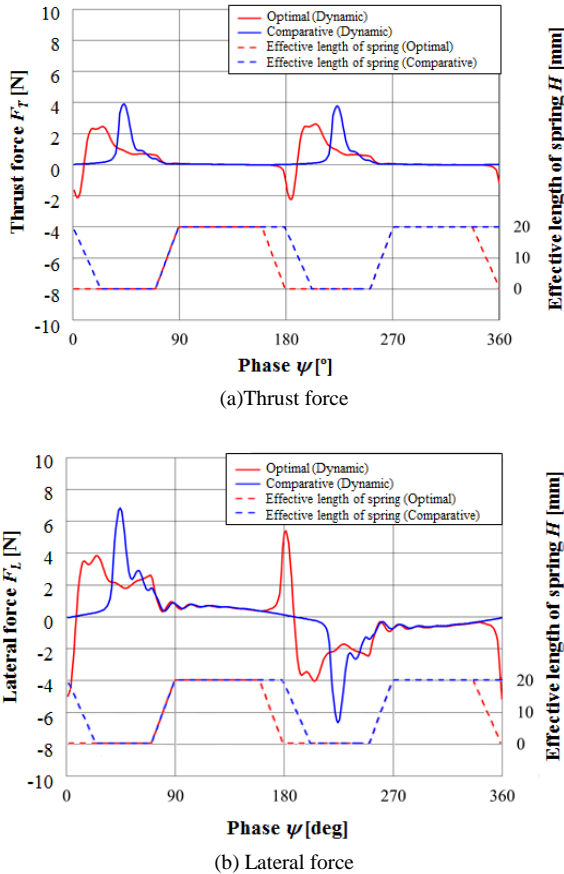


Fig. 14. Correlation between fluid forces with the effective length of the spring in optimal dynamic and comparative dynamic conditions

Table 2 Average thrust force  $\bar{F}_T$ , average required power  $\bar{P}_{in}$ , and thrust efficiency  $E$  under static and dynamic conditions

Condition	$\bar{F}_T$ [N]	$\bar{P}_{in}$ [W]	$E$
$H=3\text{mm}$ (Static)	0.330	0.204	1.615
$H=20\text{mm}$ (Static)	0.130	0.049	2.634
Comparative (Dynamic)	0.345	0.129	2.674
Optimal (Dynamic)	0.368	0.128	2.864

force is suppressed under comparative dynamic conditions, the value of the thrust efficiency is smaller than that under optimal dynamic conditions. This result suggests that it is better setting a long duration for the fin to push the fluid than setting a long duration for the fin to turn aside the fluid, as thrust efficiency is higher. The purpose of the kriging method is to maximized Eq. (1), and although a large negative thrust force was generated near phases  $\psi = 180(0, 360)^\circ$ , it has found conditions for which thrust efficiency was maximized. The argument is similar to that regarding lateral forces.

## V. CONCLUSION

In summary, a fin with a variable-effective-length spring as a mechanism to vary stiffness was modeled using ANSYS 13.0/ ANSYS Mechanical. Using this structure model and a fluid model configured under ANSYS13.0/ ANSYS CFX 13.0, a 2D fluid–structure interaction analysis was performed of the oscillations of

the fin in still water. The purpose of this research was to simulate the dynamic conditions under which the fin stiffness changed during the oscillatory motion. This simulation was achieved, and the dynamic control of the fin’s stiffness was optimized using the kriging method. The following results were obtained:

- (i) The apparent stiffness of the exposed portion of the variable-effective-length spring was represented by Young’s modulus artificially by using the settings of the physical properties available in ANSYS Mechanical.
- (ii) The improvement of the average thrust force  $\bar{F}_T$  and the evaluated value of thrust efficiency  $E$  was possible using dynamic conditions.
- (iii) Under the optimal dynamic condition obtained using the kriging method, although a large negative thrust force was generated during the latter stage of the outstroke, the positive thrust force generated was larger than that under static conditions during the instroke.
- (iv) Under optimal dynamic conditions, large positive and negative lateral forces were suppressed during the outstroke, which induced forces in the instroke.
- (v) Setting a long duration for the fin to push the fluid is better than setting a long duration for the fin to turn aside the fluid, for then the thrust efficiency is higher under dynamic conditions.
- (vi) The direction of the induced flow effecting the propulsion direction at the tip of the fin was close to that of the reverse propulsion under optimal dynamic conditions, for which the flow velocity was higher than those under static conditions.

In future work, a more detailed analysis is needed for the relationship between the design variables and the thrust characteristics of the propulsion mechanism. Also an evaluation is needed of thrust efficiency that includes consideration of the power required in controlling fin stiffness.

## Acknowledgements

This work was supported by JSPS KAKENHI Grant No. 15K16337.

## References

- [1] Triantafyllou, M. S. and Triantafyllou, G. S. , An Efficient Swimming Machine, Scientific American, Vol. 272, No. 3(1995), pp. 64–70.
- [2] Motomu, N., Kenichirou, T., and Ono, K. , Experimental study of aTwo-Joint Dolphinlike Propulsion Mechanism (2nd Report, Experiment of Self-Propelled Large Robot), Transaction of the Japan Society of Mechanical Engineering (in Japanese), Series B, Vol. 66, No. 643(2000), pp. 703–709.
- [3] Liu, J. and Hu, H. , Biological Inspiration: From Carangiform Fish to Multi-Joint Robotic Fish, Journal of Bionic Engineering, Vol. 7, No. 1(2010), pp. 35–48.
- [4] Watanabe, M., Muramatsu, K., and Kobayashi, N. , Propulsion Performance of an Aquatic Mobile Robot Using Traveling-Wave Motion of a Flexible Fin (Relationship between Propulsion Efficiency and Flow Pattern), Transaction of the Japan Society of Mechanical Engineering (in Japanese), Series C, Vol. 68, No. 665(2002), pp. 188–196.
- [5] Long, J. H., Krenitsky, N. M., Roberts, S. F., Hirokawa, J., De Leeuw, J., and Porter, M. E. , Testing biomimetic structures in bioinspired robots: How vertebrae control the stiffness of the body

- and the behavior of fish-like swimmers, *Integrative and Comparative Biology*, Vol. 51, No. 1(2011), pp. 158–175.
- [6] Takada, Y., Araki, R., Ochiai, T., Tajiri, T., and Wakisaka, T. , Effects of tail fin flexibility on propulsive performance in small fish robots (Investigation by fluid-structure interaction analysis considering elastic deformation of tail fin), *Transactions of the Japan Society of Mechanical Engineers (in Japanese), Series C*, Vol. 77, No. 778(2011), pp. 2351–2362.
- [7] Takada, Y., Nakanishi, Y., Araki, R., Nonogaki, M., and Wakisaka, T. , Effect of Material and Thickness about Tail Fins on Propulsive Performance of a Small Fish Robot, *Journal of Aero Aqua Bio-mechanisms*, Vol. 1, No. 1(2010), pp. 51–56.
- [8] Kobayashi, S., Nakabayashi, M., and Morikawa, H. , Bioinspired Propulsion Mechanism in Fluid Using Fin with Dynamic Variable-Effective-Length Spring, *Journal of Biomechanical Science and Engineering*, Vol. 1, No. 1(2006), pp. 280–289.
- [9] Nakabayashi, M., Kobayashi, R., Kobayashi, S., and Morikawa, H. , Propulsion mechanism in fluid using fin with dynamic variable-effective-length spring (Evaluation of thrust efficiency and flow-visualization around the fin), *Transactions of the Japan Society of Mechanical Engineering (in Japanese), Series B*, Vol. 73, No. 736(2007), pp. 115–123.
- [10] Nakabayashi, M., Kobayashi, R., Kobayashi, S., and Morikawa, H. , Bioinspired propulsion mechanism using a fin with a dynamic variable-effective-length spring: Evaluation of thrust characteristics and flow around a fin in a uniform flow, *Journal of Biomechanical Science and Engineering*, Vol. 4, No. 1(2009), pp. 82–93.
- [11] Nakabayashi, M., Yamazaki, W., and Kobayashi, S. , Numerical study of propulsion mechanism in fluid using fin with variable stiffness mechanics, *Transactions of the JSME (in Japanese)*, Vol. 80, No. 812(2014), pp. 1–14.
- [12] Jones, D. R., Schonlau, M., and William, J. , Efficient Global Optimization of Expensive Black-Box Functions, *Journal of Global Optimization*, Vol. 13(1998), pp. 455–492.
- [13] Yamazaki, W. and Mavriplis, D. J. , Derivative-Enhanced Variable Fidelity Surrogate Modeling for Aerodynamic Functions, *AIAA Journal*, Vol. 51, No. 1(2013), pp. 126–137.
- [14] Motomu, N. , Dynamics of Two-Joint Dolphinlike Propulsion Mechanism (6th Report, Examination by Three dimensional Panel Method into Effects Which is Unable to be Treated by Linear Theory), *Transaction of the Japan Society of Mechanical Engineering (in Japanese), Series B*, Vol. 69, No. 683(2003), pp. 39–46.
- [15] Borazjani, I. and Sotiropoulos, F. , Numerical investigation of the hydrodynamics of carangiform swimming in the transitional and inertial flow regimes, *Journal of Experimental Biology*, Vol. 211(2008), pp. 1541–58.